AMUEM 2006 - International Workshop
on Advanced Methods for Uncertainty Estimation in Measurement
Sardagna, Trento, Italy, 20–21 April 2006

Uncertainty Analysis of Measurement Principles Based on Objective Laser Speckle Correlation

Thomas Thurner and Markus Brandner
Institute of Electrical Measurement and Measurement Signal Processing
Graz University of Technology, Austria
{*thurner, brandner*}@*ieee.org*

Abstract *– Propagating uncertainty is one of the key issues in complex measurement systems. This paper addresses the propagation of uncertainty applied to the field of optical measurement systems, focusing on the objective speckle correlation (OSC) technique for strain and displacement measurement on rough surfaces in a contact-less manner. Due to the complexity of the underlying physical and electrical phenomena we apply a Monte-Carlo analysis to determine the uncertainties for a given experimental setup, and verify some of the outcomes of investigations with practical measurements under laboratory conditions.*

Keywords *– Uncertainty propagation, laser speckle correlation, objective laser speckles, optical measurement, strain and displacement measurement.*

I. INTRODUCTION

Laser speckle techniques are widely used for displacement and strain measurement in non-destructive testing and material science applications since they are very attractive due to the non-contacting operating principle and the attainable high measurement resolution. Speckle-based metrology can be divided into interferometric methods such as electronic speckle interferometry (ESPI), speckle holography and speckle shearing interferometry, and correlation-based speckle techniques such as speckle photography [1], [2]. The investigated measurement technique utilizes the properties of objective laser speckles which originate from a coherently illuminated optically rough surface. Information about the topology of the illuminated part of a specimen's surface are coded into the scattered light waves. When observing the interference of these scattered wavelets on an intensity basis in an observation plane in the far field, a speckle pattern appears which can be acquired by means of a CCD sensor. Since there is no need for imaging lenses, the observed speckles are called objective speckles. In contrast to subjective speckles observed with the help of an imaging system, each local speckle of an objective speckle pattern bears information about the topology of the *whole* illuminated surface area [3].

The described OSC technique can be utilized to measure displacement, rotation and surface strain of diffusely reflecting specimen requiring only a very basic optical setup. Since the OSC method is a non-contacting measurement principle, strain measurement on specimen with highest surface temperatures is possible – most desirable in material science applications [4], [5], [6]. Furthermore it is possible to evaluate surface strain within a very small area on the device under test (DUT), achieved by illuminating only a very small area of less than 1 mm in diameter on the specimen – this can be viewed as a *point-like measurement of strain*, which can hardly be done by alternative measurement principles [7].

A practical measurement arrangement for OSC measurement

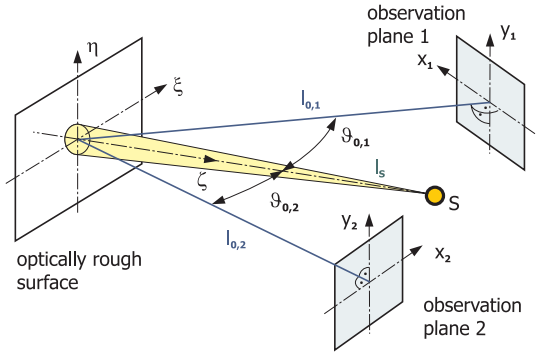

Fig. 1. Optical arrangement for strain measurement with objective speckle techniques. A laser beam illuminates a certain surface area of the specimen, producing two speckle patterns which are observed from two directions on observation planes arranged perpendicular to the observation direction. l_S is the illumination distance, l_0 the observation distance and ϑ_0 is the observation angle.

of surface strain is schematically depicted in Fig. 1, where it can be seen that the mean surface normal, the laser source, and the centers of the observation planes need to lie in the (ξ, ζ)-plane. To be able to separate the influence of surface strain (the mostly desired physical parameter) on speckle pattern movements from surface rotations and displacements, further restrictions on the geometry of the optical arrangement must be made. In particular, the symmetric arrangement of the observation planes with respect to the normal direction of the mean surface on the object under test, and the collinear alignment of

1-4244-0249-2/06/$20.00 ©2006 IEEE

the laser beam with respect to the surface normal are prominent influencing factors. Any practical measurement geometry deviates from the above restrictions and other manufacturing tolerances such as misalignment in the setup, leading to measurement uncertainties. Furthermore, the use of a not perfectly stable laser source – e.g. an unstabilized laser diode module – further causes additional uncertainties in the measurement results [8]. To our knowledge, the estimation of uncertainty in the measurement results obtained by OSC measurements has not satisfactorily been discussed within the scientific community.

II. OBJECTIVE LASER SPECKLE CORRELATION

A. Theoretical Background for OSC

A theoretical description of the objective speckle formation has been given by I. Yamaguchi [9] more than 20 years ago, where he investigated the consequences of translation, rotation, and surface strain of a coherently illuminated plane surface objective laser speckle dynamics. The mechanical changes of the illuminated surface area are described by the translation vector $\boldsymbol{\alpha} = [\alpha_\xi, \alpha_\eta, \alpha_\zeta]^T$, the rotation vector $\boldsymbol{\Omega} = [\Omega_\xi, \Omega_\eta, \Omega_\zeta]^T$, and the symmetric linear surface strain tensor

$$\breve{\varepsilon} = \begin{bmatrix} \varepsilon_{\xi\xi} & \varepsilon_{\xi\eta} \\ \varepsilon_{\xi\eta} & \varepsilon_{\eta\eta} \end{bmatrix},$$

as depicted in Fig. 2. These mechanical changes of the illuminated surface primarily lead to a speckle pattern displacement $\mathbf{a} = [a_x, a_y]^T$ in an observation plane. Secondary, the movement and microstructural change in the illuminated surface area lead to a certain degree of decorrelation in the observed speckle pattern thus introducing random noise.

Based on a modified version of the not exact theory of Fresnel diffraction [10], including several further assumptions and restrictions as outlined in [8], analytic formulae describing the desired local behavior of a speckle pattern can be derived [9]:

$$\begin{aligned} a_x = &-\alpha_\xi \left(\frac{l_0}{l_S} \frac{(e_{S\xi}^2 - 1)}{\cos\vartheta_0} - \cos\vartheta_0 \right) - \alpha_\eta \left(\frac{l_0}{l_S} \frac{e_{S\xi} e_{S\eta}}{\cos\vartheta_0} \right) \\ &- \alpha_\zeta \left(\frac{l_0}{l_S} \frac{e_{S\xi} e_{S\zeta}}{\cos\vartheta_0} + \sin\vartheta_0 \right) - \\ &- \varepsilon_{\xi\xi}\, l_0 \left(\frac{e_{S\xi}}{\cos\vartheta_0} + \tan\vartheta_0 \right) - \varepsilon_{\xi\eta}\, l_0 \left(\frac{e_{S\eta}}{\cos\vartheta_0} \right) - \\ &- \Omega_\zeta\, l_0 \left(\frac{e_{S\eta}}{\cos\vartheta_0} \right) + \Omega_\eta\, l_0 \left(\frac{e_{S\zeta}}{\cos\vartheta_0} + 1 \right), \end{aligned} \tag{1}$$

$$\begin{aligned} a_y = &-\alpha_\xi \left(\frac{l_0}{l_S} e_{S\eta} e_{S\xi} \right) - \alpha_\eta \left(\frac{l_0}{l_S} (e_{S\eta}^2 - 1) - 1 \right) - \\ &- \alpha_\zeta \left(\frac{l_0}{l_S} e_{S\eta} e_{S\zeta} \right) - \\ &- \varepsilon_{\eta\eta}\, l_0 e_{S\eta} - \varepsilon_{\xi\eta}\, l_0 \left(e_{S\xi} + \sin\vartheta_0 \right) + \\ &+ \Omega_\zeta\, l_0 \left(e_{S\xi} + \sin\vartheta_0 \right) - \Omega_\xi\, l_0 \left(e_{S\zeta} + \cos\vartheta_0 \right). \end{aligned} \tag{2}$$

The formulae describe the shift of an objective speckle pattern $\boldsymbol{a} = [a_x, a_y]^T$ in an observation plane, obtained by the geometrical arrangement depicted in Fig. 3: The mean surface of the illuminated surface area (the scattering spot on the DUT) is located in the $(\xi, \eta)-$plane in the local surface coordinate system, with the center of the illuminated spot arranged at the coordinate origin. The observation plane is located at distance l_0 from the surface, with the observation surface normal lying in the $(\xi, \zeta)-$plane of the specimen's surface coordinate system.

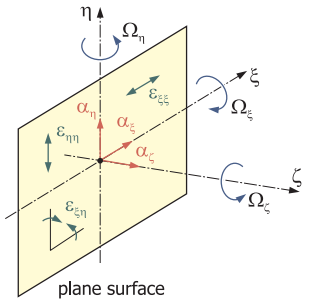

Fig. 2. Rigid body translation $\boldsymbol{\alpha}$, rotation $\boldsymbol{\Omega}$, and linear strain $\breve{\varepsilon}$ within the surface area of interest (local (ξ, η, ζ)-coordinate system).

The observation plane is oriented perpendicular to the observation direction, such that the $y-$axis of the observation coordinate system is parallel to the $\eta-$axis, and the $x-$axis lies in the $(\xi, \zeta)-$plane. Thus the distance l_0 and the angle ϑ_0 between the mean surface normal (i.e. the $\zeta-$axis) and the observation direction describe the given observation position. The illuminating coherent point source is located at distance l_S in direction $\boldsymbol{e}_S = [e_{S\xi}, e_{S\eta}, e_{S\zeta}]^T$ from the origin, where collimated illumination can be introduced by $l_S \to \infty$.

The derived formulae hold for observation in the far-field, i.e. the observation distance l_0 by far exceeds the size of the scattering spot D on the surface $l_0 \gg D$, but only for small surface displacement compared to D, small linear surface strain and limited rotation. Furthermore, the spatial extent of the observation plane needs to be much smaller than the observation distance l_0 – such that the properties of the objective speckles remain unchanged within the observation plane.

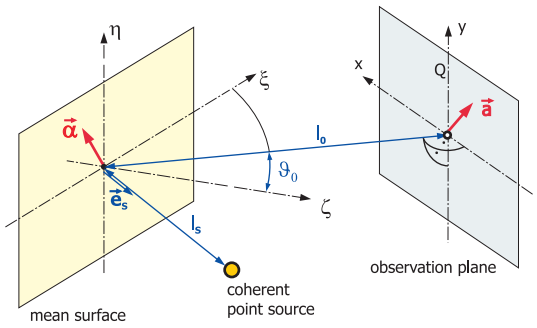

Fig. 3. Geometry for the description of speckle displacement due to surface displacement, rotation and strain.

B. Practical Setup for Strain and Displacement Measurement

The described change in the speckle patterns can be used to estimate surface displacement, strain, and rotation. A closer look on Eqs. 1 and 2 reveals, that at least 5 different observation locations are needed to estimate all 9 surface parameters out of

the observed speckle pattern displacements. The relationships drastically reduce in complexity when collimated illumination ($l_S \to \infty$) and observation from two symmetrical observation directions are introduced by the so-called single-beam OSC setup as schematically sketched in Fig. 1. The speckle pattern shifts in the two observation planes 1 and 2 are given by $\boldsymbol{a_1} = [a_{x,1}, a_{y,1}]^T, \boldsymbol{a_2} = [a_{x,2}, a_{y,2}]^T$, where the differential shift $\Delta a_x, \Delta a_y$ and the average shift $\overline{a_x}, \overline{a_y}$ are given by

$$\Delta a_x = a_{x,1} - a_{x,2} = -2\varepsilon_{\xi\xi}\, l_0 \tan\vartheta_0 - 2\alpha_\zeta \sin\vartheta_0\,, \tag{3}$$

$$\Delta a_y = a_{y,1} - a_{y,2} = -2\varepsilon_{\xi\eta}\, l_0 \sin\vartheta_0 + 2\Omega_\zeta\, l_0 \sin\vartheta_0\,, \tag{4}$$

$$\overline{a_x} = \frac{1}{2}(a_{x,1} + a_{x,2}) = \alpha_\xi \cos\vartheta_0 + \Omega_\eta\, l_0\,(\cos\vartheta_0 + 1)\,, \tag{5}$$

$$\overline{a_y} = \frac{1}{2}(a_{y,1} + a_{y,2}) = \alpha_\eta - \Omega_\xi\, l_0\,(\cos\vartheta_0 + 1)\,. \tag{6}$$

Most desirable in material science applications is the measurement of in–plane surface strain components of a specimen. Especially for tensile tests the measurement of the uniaxial surface strain in direction of the mechanical load $\varepsilon_{\xi\xi}$ needs to be measured. The desired strain component can be obtained out of Eq. 3 by

$$\varepsilon_{\xi\xi} = -\frac{\Delta a_x}{2 l_0 \tan\vartheta_0} + \frac{\alpha_\zeta \cos\vartheta_0}{l_0}\,. \tag{7}$$

The speckle patterns are acquired by 2D imaging cameras, introducing spatial quantization and integration as well as intensity quantization and temporal integration. The shift in each speckle pattern (the spatial pattern shift between two consecutive image acquisitions in the same observation plane) is estimated by a correlation–based algorithm from the digitized speckle patterns [8].

Eq. 7 is used in almost all practical realizations of the described OSC principle for strain measurement. It is evident that a major drawback of the principle is the dependence of Δa_x on known or unknown out–of–plane surface displacement α_ζ in the $\zeta-$direction, which need to be measured by alternative principles or must remain small to be able to neglect this influence on the measurement result [8]. In the following we will discuss the the topic of measurement uncertainty introduced by an uncertain or misaligned geometry and the data acquisition and processing.

III. UNCERTAINTY IN OSC

To reduce the complexity we focus our investigation to obtain an uncertainty budget only for measurement of in-plane surface strain $\varepsilon_{\xi\xi}$ and displacement in the $\xi-$direction, since these measures are most important in practical applications of the OSC principle. Fig. 4 outlines the processing steps involved in estimation of the desired horizontal displacement and strain parameters. Subsequently we comment on each processing step.

A. Sensor Geometry

For deviations from the ideal geometry of the single-beam setup described above, Eqs. 1 and 2 have to be used for each observation geometry (i.e. positions of light source, illuminated surface, and observation plane as indicated in Fig. 3). After the combination of two observation geometries – as needed for strain and displacement measurement – into a full sensor model, the following influencing factors contribute to the differential speckle shift Δa:

$$\begin{aligned}\boldsymbol{\Delta a} = \boldsymbol{f}\,(&\boldsymbol{\alpha}, \boldsymbol{\Omega}, \breve{\varepsilon}, l_{0,1}, \vartheta_{0,1}, l_{0,2}, \vartheta_{0,2},\\ &\boldsymbol{e_{S,1}}, \boldsymbol{e_{S,2}}, l_S, \boldsymbol{R_{0,1}}, \boldsymbol{R_{0,2}}, \boldsymbol{R_{DUT}}\,)\,,\end{aligned} \tag{8}$$

where $\boldsymbol{R_{DUT}}$, $\boldsymbol{R_{0,1}}$ and $\boldsymbol{R_{0,2}}$ describe rotations of the specimen's mean surface and the observation planes 1 and 2, and $\boldsymbol{e_{S,1}}, \boldsymbol{e_{S,2}}$ are the relative positions of the illuminating laser source as seen from the corresponding observation plane.
A reduction in complexity can be obtained by neglecting influences from non-ideal alignment of the inspected surface with respect to the two observation planes and the neglect of possible tilts in the observation planes and the DUT's surface with respect to their nominal positions: in this case $\boldsymbol{R_{DUT}} = \boldsymbol{R_{0,1}} = \boldsymbol{R_{0,2}} = \boldsymbol{I}$ and both observation planes see the same position of the light source, i.e. $\boldsymbol{e_{S,1}} = \boldsymbol{e_{S,2}} = \boldsymbol{e_S}$. All these simplifications are justified when the optical setup has been carefully aligned according to the ideal sensor geometry. Remaining parameters influencing the uncertainty in the optical setup are:

- Positioning of the observation planes: $l_{0,1} \neq l_{0,2}$ and $\vartheta_{0,1} \neq \vartheta_{0,2}$
- Illumination direction: $\boldsymbol{e_S} \neq [0,0,1]^T$
- Non-collimated illumination: $l_S \leq \infty$.

Due to the chosen simplifications the relevant speckle dynamics for strain and displacement measurement in the $\xi-$direction appear within the $(\xi,\zeta)-$plane only.

B. Image Acquisition

The acquisition of the laser speckle patterns is performed by two identical digital CCD cameras of Type DMK-21BF04 with a $640 \times 480\,\text{pixel}^2$ CCD detector array and a pixel size of $5.6 \times 5.6\,\mu\text{m}^2$. The acquired image data is quantized to obtain 8 bit digital images.
The transform of a spatially and temporally continuous intensity information in the plane of the CCD array to digital image data clearly influences the information content of the data. The intensity-to-voltage and analog-to-digital conversion within the CCD sensor produces additional noise – so-called electronic noise, comprised from detector noise (photon shot noise, dark current noise, fixed pattern noise and reset noise), amplifier noise ($1/f$-noise) and quantization noise. All these noise components determine the Signal-to-Noise-Ratio (SNR) of the used camera. This additional noise clearly contributes to decorrelation of the acquired speckle patterns. Although, for the used camera these influences need to be incorporated only for very low light conditions. Under normal light conditions as it is the case for OSC measurements, the decorrelation due to electronic noise can be characterized by a correlation factor in excess of 0.99 [11], justifying the neglect of these influences. The influences of temporal intensity integration during the image acquisition can be neglected when the movement of the

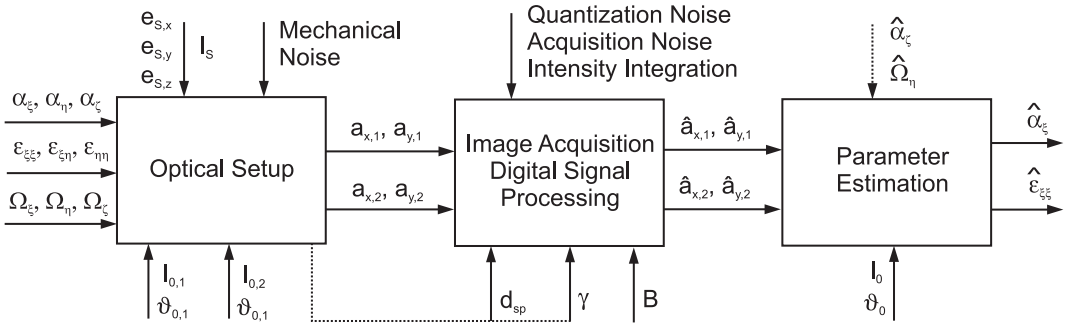

Fig. 4. Parameters and noise sources determining measurement uncertainty of OSC principles. The optical setup transforms mechanical deformation of the DUT ($\boldsymbol{\alpha}, \boldsymbol{\omega}, \breve{\varepsilon}$) into 2D displacement ($\boldsymbol{a_1}, \boldsymbol{a_2}$) of two speckle patterns acquired via two cameras, which are used to estimate the desired surface displacement α_ξ and linear surface strain $\varepsilon_{\xi\xi}$. The measurement process can be divided into three separate parts, the optical setup producing speckle pattern shifts in the observation planes correlated to mechanical deformation on the surface, the image acquisition and signal processing estimating the speckle shift in the observation plane, and the parameter estimation calculating the desired mechanical measures strain and displacement out of the speckle pattern shifts.

observed speckle patterns during the period of intensity integration in the CCD camera remain small compared to the given pixel size. The sampling of the continuous intensity distribution is done by the regularly spaced pixel array. The structural size within a fully developed speckle pattern is limited in case of a uniformly illuminated circular area of diameter D and our chosen optical setup, and determined by the minimum speckle sizes [8]

$$d_{min,x} = \frac{\lambda}{D\cos\vartheta_0} l_0 \quad , \, d_{min,y} = \frac{\lambda}{D} l_0 \tag{9}$$

in the directions of the sampling grid. Given pixels of size p_x, p_y, the sampling theorem is fulfilled when $d_{min,x} > 2p_x$ and $d_{min,y} > 2p_y$. Clearly, any violation of the sampling theorem introduces systematic errors into the measurement. For the given optical setup the allowed range for the diameter of the illumination spot D can be obtained as

$$D < \frac{\lambda l_0}{2p_x \cos\vartheta_0} \approx 23\text{mm} \, , \tag{10}$$

where the parameters of the chosen optical setup were used to determine the limit for our experiments.

Spatial sampling of the intensity distribution comes with spatial integration within the active area of each pixel. For a high fill factor of the pixel array – which is necessary for high sensitivity of the camera – the high frequency components close to half the sampling frequency of the speckle pattern are attenuated. This influence can be neglected in our case due to the relatively low spatial frequency of the speckle pattern obtained by an illumination spot size of $D = 2 \ldots 6\,\text{mm}$ during our experiments.

C. Signal Processing

Speckle pattern displacements between consecutive images bear the desired measurement information within. A straightforward method of determining the speckle pattern displacement is the calculation of the 2D cross–correlation function of two speckle images and the search for the peak position of the obtained correlation function. We use a modified version of cross-correlation, which is the normalized cross-covariance function (CCF) of the reference image $I_r[m,n]$ of size $M_r \times N_r$ and the template image $I_t[m,n]$ of size $M_t \times N_t$

$$c[k,l] = \tag{11}$$
$$= \frac{\sum_{m=0}^{M_r-1}\sum_{n=0}^{N_r-1} \left[I_r[m,n] - \overline{I_r}\right]\left[I_t[m-k,n-k] - \overline{I}_t\right]}{\sqrt{\sum_{m=0}^{M_r-1}\sum_{n=0}^{N_r-1} \left|I_r[m,n] - \overline{I_r}\right|^2 \cdot \sum_{m=0}^{M_t-1}\sum_{n=0}^{N_t-1} \left|I_t[m,n] - \overline{I_t}\right|^2}}$$

where it is assumed that the template is smaller than the reference, $M_r > M_t$ and $N_r > N_t$. The result is a cross-covariance function of size $(M_r - M_t + 1) \times (N_r - N_t + 1)$, containing the correlation peak where the shifted template image best matches the corresponding area in the reference image. The normalization of the CCF ensures that the maximum value of the CCF – the value at the position of the peak in the CCF – corresponds to an estimate of the correlation coefficient γ between the shifted template and the reference image. A sinc-interpolation of the CCF by zero-padding in the Fourier domain [8] is applied to achieve sub-pixel resolution.

The uncertainty of a correlative speckle pattern displacement estimation as described above has been determined for speckle patterns with a correlation factor γ in [12],[13] as

$$u_{CCF,x} = k\frac{d_{sp,x}^2}{B_x}\sqrt{\frac{1-\gamma}{\gamma}}, \tag{12}$$

where k is a constant factor determined as $k = \sqrt{2/\pi}/1.2 \approx 0.7$ as outlined in [13]. B_x is the width of the image template, given by $B_x = M_t p_x$, and $d_{sp,x}$ is the average speckle size on the detector in $x-$direction, determined by [8],[3]

$$d_{sp,x} = 1.22\frac{\lambda}{D\cos\vartheta_0} l_0. \tag{13}$$

Within a real measurement the value of the correlation coefficient can be obtained by evaluating the peak value of the normalized cross-covariance function CCF for each estimation of speckle displacement.

For our estimation of uncertainty within the signal processing scheme we follow the ideas in [13] applied to the free space geometry of the OSC principle, which allows the estimation of

the correlation coefficient γ – also known as the Yamaguchi correlation factor – by

$$\gamma = \left(\frac{\Theta - sin\Theta}{\pi} \right)^2 \quad , \quad \Theta = 2 \arccos \frac{|\Delta|}{D}. \qquad (14)$$

Δ is the relative shift of the specimen's surface with respect to the illumination spot on the surface of Diameter D. The decorrelation δ in the acquired speckle patterns is related to the correlation coefficient by $\delta = 1 - \gamma$. The primary source of *objective* speckle pattern decorrelation is the in-plane displacement of the specimen's surface with respect to the illumination spot. Other influencing factors like surface strain, surface tilt, and the limited speckle size in the out-of-plane direction can be neglected [8].

IV. UNCERTAINTY ESTIMATION

For a practical setup the uncertainty associated to the measurement result has been evaluated using both a simulation environment and a real-world OSC setup.

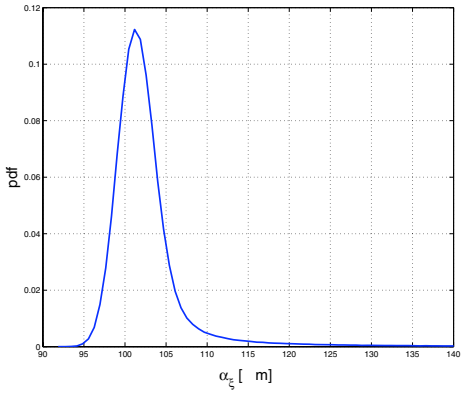

Fig. 5. Estimated pdf obtained from a Monte-Carlo analysis for uncertain parameters in the measurement of in–plane surface displacement $\hat{\alpha}_\xi$ and a true displacement of $\alpha_\xi = 100\,\mu$m.

A. Monte-Carlo Simulations

The complex measurement model and the diversity of influencing parameters render an analytic treatment of the propagation of uncertainty as suggested by the GUM [14] impossible for all but the most trivial sensor geometries. We use probability density functions (pdfs) as information carriers for the relevant input parameters of a Monte-Carlo (MC) simulation. The parameters covered by the simulation are:

1. *Laser Source*: Both position and distance of the laser source are subjected to variations. Emphasis is put on imperfect laser collimation which results in large variations of the source distance l_s. From experience we allow the distance to uniformly take on any value in the interval $[1, 100)$ m.
2. *Sensor*: Both cameras can only be setup at a certain level of accuracy. We allow independent uniform deviations of ± 1 mm in position and $\pm 1^\circ$ in orientation for each camera.
3. *Mechanical Vibrations*: Vibration of the whole sensor setup impacts on the sensor uncertainty. In our simulation a random motion of the DUT in 3D subjected to a Gaussian distribution with independent standard deviations of $\sigma_{x,y,z} = 1\,\mu m$ for each axis is assumed.
4. *Image Processing*: The detection performance depends on the decorrelation of the speckle patterns. In our simulations an additive Gaussian component with a standard deviation as given by Eqn. 12 is used.

In order to obtain comparable results the sensor geometry of our laboratory interferometer is adopted. In particular, our setup is defined by the parameters $D = 3\,$mm, $l_0 = 0.145\,$m, $\vartheta_0 = \pm 45^\circ$, $\boldsymbol{e_S} = [0, 0, 1]$, and a HeNe-Laser with wavelength $\lambda = 632.8\,$nm and a collimated beam expanded to a diameter of $3\,$mm. Fig. 5 depicts the simulated pdf of the measured displacement for a true displacement of $\alpha_\xi = 100\,\mu$m and a surface strain of $\epsilon_{\xi\xi} = 20\,$ppm. During this simulation $M = 10^6$ samples of the displacement are computed using the above listed input parameter pdfs. The resultant pdf deviates from the standard Gaussian pdf by a long tail towards larger displacements. This deviation is caused by the imperfect configuration of the light source. The associated strain estimate as shown in Fig. 6 exhibits no significant bias and shows good performance.

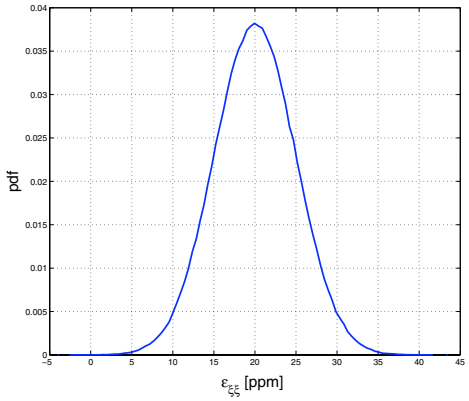

Fig. 6. Estimated pdf obtained from a Monte-Carlo analysis for uncertain parameters in the measurement of in–plane surface strain $\hat{\varepsilon}_{\xi\xi}$ and a true strain value of $\varepsilon_{\xi\xi} = 20\,$ppm.

B. Experiments

In our laboratory OSC setup the DUT is an aluminum plate with an optically rough surface, mounted onto a motorized 3D translation stage with a resolution and repeatability of $0.1\,\mu$m, allowing for displacement measurements under sufficiently controlled laboratory conditions. The main purpose of the practical experiments is the evaluation of the results from our Monte-Carlo Simulation. The solid line in Fig. 7 shows the standard deviation σ_α for displacement measurements obtained from evaluating 100 independent measurement cycles, each consisting of 200 surface displacements from $\alpha_\xi = 0, 2, \ldots, 200\,\mu$m, plotted over the true surface displacement. All measurement cycles have been carried out with the

identical optical setup, only the illuminated surface area has been changed such that the speckle patterns for each measurement cycle are independent from each other. For larger surface displacements the standard deviation in the displacement measurement increases. Comparing these experimental results with values obtained from our simulation (dotted line in Fig. 7) reveals some significant differences between them. Although both results are in the same order of magnitude and show similar dependencies from the true surface displacements, the plotted curves are not in perfect agreement as discussed below.

Fig. 8 shows the plot of correlation coefficients γ_1 and γ_2 as a

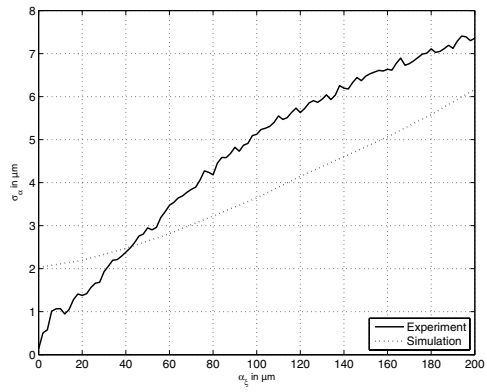

Fig. 7. Standard deviation in a speckle pattern shift estimation, obtained from 100 experiments.

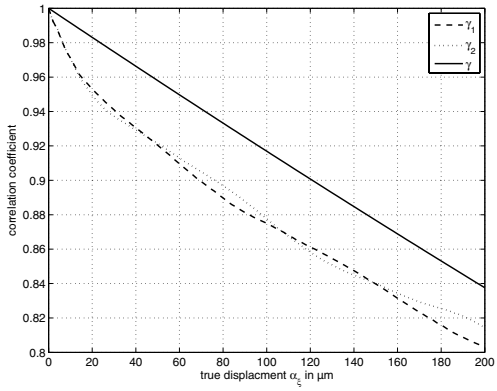

Fig. 8. Comparison of correlation coefficients γ_1, γ_2 obtained from evaluating the CCF from speckle patterns acquired in observation planes $1, 2$ during surface displacement from $\alpha_\xi = 0 \ldots 200\,\mu$m, with the theoretical value of the correlation factor γ for the given displacements.

dotted and a dashed line. An average over 100 statistically independent measurement cycles each comprising 200 displacement measurements in the range of $\alpha_\xi = 0, 2, \ldots, 200\,\mu$m are shown. Comparing these coefficients with the theoretical value calculated out of Eq. 12 and plotted as solid line over the true surface displacement, shows that our model for estimating the correlation coefficient does not sufficiently well fit to the underlying physical phenomena. For small displacement values the measured correlation factor decreases much faster with increasing displacement as the theoretical, whereas for displacements larger than $80\,\mu$m both the experimental and the theoretical correlation factor show the same dependence on the true displacement, although the real-world estimation of the correlation factor remains below the theoretical value with a bias of approx. 0.04. Recalling the comparison of standard deviations in measurement results and simulation results discussed above, the observed relationships explain the differences between experiment and simulation: For small displacements, the dominating influence factors in the Monte-Carlo simulation are assumed surface vibrations, leading to higher values than the values obtained for our laboratory setup. For larger displacement values, the simulation results show the same dependence on surface displacements as the experimental results, but remain smaller due to the use of the theoretical correlation coefficient γ for estimation of the uncertainty in the signal processing.

V. CONCLUSION

Objective laser speckle correlation methods are used to directly measure linear surface strain on specimen with a diffusely scattering surface. An analytic investigation of the performance of OSC setups is exceedingly difficult given the complex measurement model and the different natures of the contributing parameters. In this work we investigate the performance of an OSC setup using Monte-Carlo simulations and propagations of uncertainties as suggested by the GUM.

Experimental validations indicate the feasibility of this approach. A further refinement of the measurement model and associated parameter uncertainties is a current topic of research at our institution.

REFERENCES

[1] R. S. Sirohi, Ed., *Speckle Metrology*. New York: Marcel Dekker, Inc., 1993.

[2] P. K. Rastogi and D. Inaudi, Eds., *Trends in Optical Non–Destructive Testing*. Kidlington, Oxford, UK: Elsevier Science, Ltd., 2000.

[3] J. W. Goodman, "Statistical properties of laser speckle patterns," in *Laser Speckle and Related Phenomena*, 2nd ed., J. C. Dainty, Ed. Berlin: Springer–Verlag, 1984, pp. 9–75.

[4] T. Thurner, S. C. Schneider, and B. G. Zagar, "Laser–Speckle–Dehnungsmessung und deren Anwendung in der Materialwissenschaft," *tm — Technisches Messen*, vol. 02/2003, no. 70, pp. 71–78, 2003.

[5] P. Zimprich, S. C. Schneider, M. Kastner, and B. Zagar, "New developments in laser speckle strain measurement techniques," *Proceedings of ODIMAP IV*, 2004.

[6] S. C. Schneider, Y. Gautam, and B. G. Zagar, "Application of a locally operating laser–speckle strain sensor," *IEEE Transactions on Instrumentation and Measurement*, vol. 52, no. 4, pp. 1025–1029, 2003.

[7] T. Thurner and P. Wilksch, "A laser speckle sensor for single–point measurement of strain," *Proceedings of the 19th IEEE Instrumentation and Measurement Technology Conference*, pp. 741–745, 2002.

[8] T. Thurner, "Local strain measurement by objective laser speckle technique," PhD Thesis, Graz University of Technology, 2004.

[9] I. Yamaguchi, "Speckle displacement and decorrelation in the diffraction and image fields for small object deformation," *Optica Acta*, vol. 28, no. 10, pp. 1359–1376, 1981.

[10] J. W. Goodman, *Introduction to Fourier Optics*, 2nd ed. McGraw–Hill, New York, 1996.

[11] T. Fricke-Begemann, "Optical measurement of deformation fields and surface processes with digital speckle correlation," Ph.D. dissertation, Universität Oldenburg, 2002.

[12] M. Sjödahl, "Accuracy in electronic speckle photography," *Applied Optics*, vol. 36, pp. 2875–2885, 1997.

[13] ——, "Digital speckle photography," in *Digital Speckle Pattern Interferometry and Related Techniques*, P. K. Rastogi, Ed. John Wiley and Sons, 2001.

[14] *Guide to the Expression of Uncertainty in Measurement*. Genève, Switzerland: International Organization for Standardization (ISO), 1995.